Compositional Dependence of Cation Impurity Gettering in $Hg_{1-x}Cd_xTe$

JOSÉ L. MELÉNDEZ, JOHN TREGILGAS, and JOHN DODGE

Corporate Research, Texas Instruments Inc., Dallas, TX 75265

C.R. HELMS

Department of Electrical Engineering, Stanford University, Stanford, CA 94305

Cation impurity gettering in $Hg_{1-x}Cd_xTe$ is described in the context of process models which include the interactions of the impurities and the dominant native point defects. Experimental results are presented using secondary ion mass spectroscopy (SIMS) profiles of Au redistribution in $Hg_{1-x}Cd_xTe$ (x = 0.2,0.3,0.4) following Hg anneals and ion mills, which are processes known to inject excess Hg interstitials. In either process, the IB impurity distributes preferentially to high vacancy regions. The junction depth of the low to high impurity transition is determined by SIMS. For Hg-rich anneals of Au-doped high vacancy concentration material, the impurity junction behavior with respect to anneal time and temperature is compared to that expected for type converted electrical junctions in vacancy-only material. For milled Au-doped $Hg_{0.7}Cd_{0.3}Te$ with a high vacancy concentration, the impurity junction depths are approximately proportional to the amount of material removed, as was the case with x = 0.2 material. Hg anneal type-conversion rates are found to have a strong compositional dependence which compares favorably with the strong self-diffusion coefficient dependence on x-value. In contrast, the mill conversion rate has a weak x-value dependence. Effects of trace vs dominant Au levels compared to the background vacancy concentration are quantified. True decoration of intrinsic defect processes requires [Au]<<[Cation Vacancies].

Key words: Defect interactions, HgCdTe, impurity gettering, native point defects

INTRODUCTION

Diffusion experiments in $Hg_{1-x}Cd_xTe$ have traditionally focused upon x = 0.2 material for long wavelength infrared (LWIR) imaging applications. Investigation of the existence region and of fundamental diffusion phenomena such as Hg self-diffusion and type-conversion of vacancy doped material are well documented for LWIR material.[1-11] Indeed, this relatively complete information set has been instrumental in the development of comprehensive point defect models to describe diffusion in $Hg_{0.8}Cd_{0.2}Te$.[12-15] However, these models do not quantitatively treat mid-wave (MWIR, x = 0.3) nor short-wave (SWIR, x = 0.4) $Hg_{1-x}Cd_xTe$.[12] This limitation is due in large part to the incomplete diffusion characterization of the x ≠ 0.2 compositions available in the literature. In addition to the native point defect physics, interaction mechanisms of impurities such as Au and Cu have not been extensively investigated for these shorter wavelength materials. By comparison, group IB cation impurity redistribution in $Hg_{0.8}Cd_{0.2}Te$ has been studied in detail for Hg anneals and ion etching.[14,16] Group IB doped LWIR material has demonstrated promise as the base material for high performance, stable ion implanted homojunctions. In this report, we will present experimental and modeling results for the redistribution of IB cation impurities in MWIR and SWIR $Hg_{1-x}Cd_xTe$. These results will be contrasted to what is observed experimentally in LWIR material. In addition, the differences observed will be discussed in the context of anticipated variable x dependencies based upon Hg self-diffusion data.[3]

(Received October 4, 1994; revised January 15, 1995)

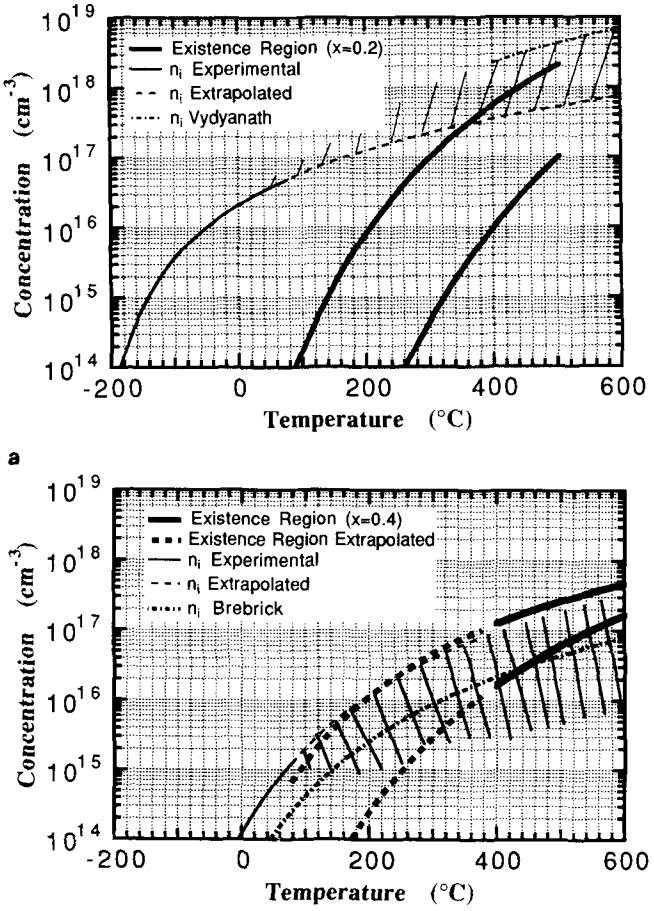

Fig. 1. Comparison of intrinsic carrier concentrations and phase limits at processing temperatures for compositions of (a) x = 0.2 and (b) x = 0.4.[1,17,18] The existence region is bound by the Hg and Te-saturated conditions from low to high vacancy concentration, respectively.

REVIEW OF POINT DEFECT KINETICS MODELING

Process models which define point defect interactions and quantify macroscopic diffusion phenomenon in LWIR material have previously been presented and discussed in detail.[12–14] These models are based on continuity equations which track the motion of each point defect by diffusion or drift, and terms which define the generation and recombination (G-R) processes. The G-R terms are based upon first order reaction kinetic descriptions of the dominant quasi-chemical reactions between the important point defects. In describing group IB impurities, the four-point defect species of interest are the Hg interstitials, cation vacancies, impurity interstitials, and substitutional impurities. The interactions of interest are the Frenkel, Frank-Turnbol, and kickout. The Frenkel reaction involves the recombination of Hg interstitials and cation vacancies or the generation of these in the reverse direction by having a Hg on a cation site move into an interstitial position. The Frank-Turnbol interaction is similar to the Frenkel, except it involves Au instead of Hg. The kickout mechanism drives substitutional Au off of its site through a "kickout" interaction with a Hg intertitial. In the reverse direction, Au interstitials "kickout" substitutional Hg. In LWIR material, drift terms are typically neglected since the relatively small bandgap (0.12 eV) results in intrinsic material under most process conditions.

Discussions in Refs. 13 and 14 have begun to outline the kinetic formalisms for variable composition systems. The key differences in the models necessary for shorter wavelength material regard the need to quantify the compositional dependence of the interaction parameters and the point defect diffusion coefficients, since the specific kinetics and thermodynamics are undoubtedly functions of composition. Drift terms to provide for ionized point defect motion and corresponding built-in electric fields are necessary since the material may not be intrinsic at typical process temperatures. In addition, the kinetic description and solution is complicated by gradients in composition, though these are neglected in the present discussion since the materials under investigation are homogeneous. A modeling approach for the general x-value system has been described in Ref. 14, where we developed a set of continuity equations for the interdiffusion problem. Perhaps the most significant barrier is the lack of a complete experimental database in the literature for $x \neq 0.2$ material, though several investigators have provided some of the necessary information.[1,3,17,18]

The present understanding of the intrinsic carrier concentrations and phase limits is summarized for x = 0.2 and 0.4 material in Figs. 1a and 1b, respectively. The thick lines are the phase limits plotted as two times the respective vacancy concentrations (assuming doubly ionized vacancies). The thin lines are various determinations of the intrinsic carrier concentrations. The measured intrinsic carrier concentrations are given by the thin solid lines below 80°C.[19] The dashed extensions are extrapolations of an empirical fit to the lower temperature data. As discussed in Ref. 14, the pressure dependence near the Te-saturated limit may be used to determine the intrinsic carrier concentration based on equilibrium point defect relationships. The upper dot-dashed curve in Fig. 1a was determined by Vydyanath utilizing such an analysis.[1] It is not clear why Vydyanath's intrinsic carrier concentrations are much higher than the extrapolation of the low temperature experimental data. The uncertainty is indicated in the figure by the shaded region. Based on a similar study of the x = 0.4 phase limits above 400°C, Vydyanath determined that the material was extrinsic in all cases.[17] This restricts the intrinsic carrier concentrations to values below the lower dot-dashed curve calculated by Brebrick and shown in Fig. 1b.[18] However, there is some question as to the accuracy of Brebrick's calculations, since they do not match the measured intrinsic carrier concentrations at room temperature. Vydyanath's intrinsic carrier concentrations also fall far below the extrapolated low temperature experimental results. The uncertainty is roughly indicated by the shaded area. The intrinsic carrier concentra-

tions at process temperatures will need to be better defined in order to quantify electric field effects during processing.

In addition to establishing the phase limits for other x-values, type-conversion analyses in these materials will also be required in order to resolve the Hg interstitial and vacancy diffusion components. The Au gettering results presented in this paper for Hg-rich anneals indicate that the type-conversion rate in x = 0.4 material is substantially reduced. This is consistent with the much smaller Hg-rich self-diffusion coefficients reported by Archer et al. for x = 0.4 material.[3]

RESULTS AND DISCUSSION

In this section, we will present and discuss the experimental results of Au gettering experiments in $Hg_{1-x}Cd_xTe$ (x = 0.2,0.3,0.4). The samples are liquid phase epitaxy (LPE) films grown from an indium counterdoped melt on Au-doped, CdZnTe lattice matched substrates. Extrinsic P-type doping of the LPE layer was achieved through a post-growth annealing schedule which ultimately results in a low background vacancy concentration ($\approx 10^{13}$ cm^{-3}). The high background vacancy levels are set through subsequent Hg poor anneals using a Te-rich capping layer. The capping layer and several microns of $Hg_{1-x}Cd_xTe$ are then stripped by wet etching, prior to the Hg interstitial injection process.

The Au profiles are measured by secondary ion mass spectroscopy (SIMS) using 14.5 keV Cs ions with a resulting material etch rate of roughly 30Å/s. While it has been established that ion milling can significantly alter the point defect densities in $Hg_{1-x}Cd_xTe$, this process typically utilizes Ar ions at a much lower energy of 0.5 keV. The validity of the SIMS technique in measuring the actual Au distributions in high concentration regions has previously been established.[16] However, the low levels observed in near surface regions depleted of Au, are believed to be an artifact resulting from kinetic gettering to the surface of some Au during the SIMS etch.[16]

Gettering Dependence on Au Concentration (x = 0.2)

The use of extrinsic impurity gettering to decorate underlying point defect processes and distributions is not new. In 1983, Bubulac et al. reported gettering of Li to implant damage, inclusions, and cation vacancies in LWIR and MWIR material.[20] Indeed, these authors suggested the use of Li as an analytical tool for understanding junction formation processes, which is the subject of the present investigation using Au, though Au itself is of interest for device applications, since it has important implications for extrinsically doped photodiodes. Schaake et al. used Cu in LWIR material to quantify type conversion rates as well as the Hg-rich phase limits at low temperature (200°C) through equilibrium point defect relationships.[2,21] More recently we have used Au to study Hg annealing, ion milling, and ion implantation in LWIR material.[14,16]

For the temperatures used in our experiments, the vacancy diffusion contribution to the junction profile is likely negligible.[12-14] The intrinsic point defect parameter values may be calculated using the SUMerCad simulator or the relationships presented in Ref. 12. Neglecting vacancy diffusion, in the steady state limit of the kinetic formulation,[14,21]

$$\frac{x_j^2}{t} = \frac{2 D_i i_R}{f v_o} . \quad (1)$$

where x_j is the junction depth, t is the Hg anneal time, D_i is the Hg interstitial diffusivity, i_R is the Hg-rich interstitial concentration, v_o is the initial vacancy concentration, and f is the interstitial sink factor. If only vacancies consume interstitials, then f = 1. If extended defects consume Au interstitials without liberating Hg interstitials, then the incoming Hg interstitials must fill the original vacancies plus vacated Au sites for the junction to progress. In addition, if extended defects consume Hg interstitials, then f is given by,

$$f v_o = v_o + [\text{Net Au interstitials consumed by non-Hg interstitial liberating defects}] + [\text{Net H interstitials consumed by nonvacancy defects}], \quad (2)$$

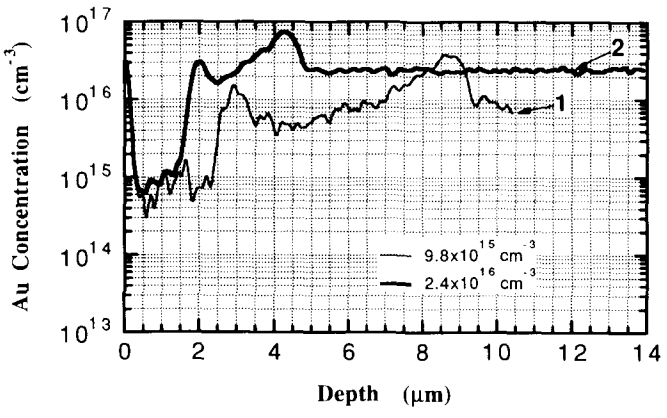

a

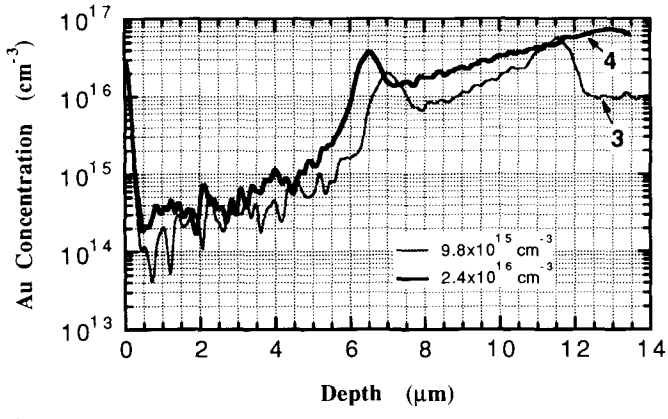

b

Fig. 2. Effect of Au concentration on redistributed Au profiles for (a) 175°C for 1h and (b) 205°C for 1h Hg anneals of 300°C Te equilibrated $Hg_{0.8}Cd_{0.2}Te$. The sample numbers are identified in the figure and can be referenced in Table I.

Table I. Summary of Initial Te-Rich Equilibration, Hg Anneal Conditions, and Junction Depths Determined from Au SIMS Profiles for all Samples

Sple.	x-value	Au Conc. (cm^{-3})	Estimated Vacancy Conc. (cm^{-3})	Te Equilibrium Temp. (°C)	Hg Anneal Temp. (°C)	Hg Anneal Time (h)	1/2 Max Junction Depth (μm)	x_j^2 v/2t (cm^{-1}/s)	f
1	0.2	9.8×10^{15}	4.8×10^{16}	300	175	1	2.5	4.2×10^{5}	2.79
2	0.2	2.4×10^{16}	4.8×10^{16}	300	175	1	1.75	2.0×10^{5}	5.85
3	0.2	9.8×10^{15}	4.8×10^{16}	300	205	1	6.8	3.1×10^{6}	2.65
4	0.2	2.4×10^{16}	4.8×10^{16}	300	205	1	5.95	2.4×10^{6}	3.43
5	0.2	1.8×10^{16}	4.8×10^{16}	300	175	1	2.55	4.3×10^{5}	2.72
6	0.2	1.8×10^{16}	4.8×10^{16}	300	205	1	6.4	2.7×10^{6}	3.05
7	0.2	2×10^{16}	1.2×10^{17}	350	205	1	4.4	3.2×10^{6}	2.57
8	0.3	3×10^{16}	8×10^{16}	350	205	4	5.5	8.8×10^{5}	—
9	0.3	3×10^{16}	8×10^{16}	350	205	16	12.0	1.0×10^{6}	—
10	0.3	3×10^{16}	8×10^{16}	350	225	4	9.0	2.2×10^{6}	—
11	0.4	9×10^{17}	4×10^{16}	350	205	4	1.0	1.4×10^{4}	—
12	0.4	9×10^{17}	4×10^{16}	350	205	16	2.05	1.5×10^{4}	—

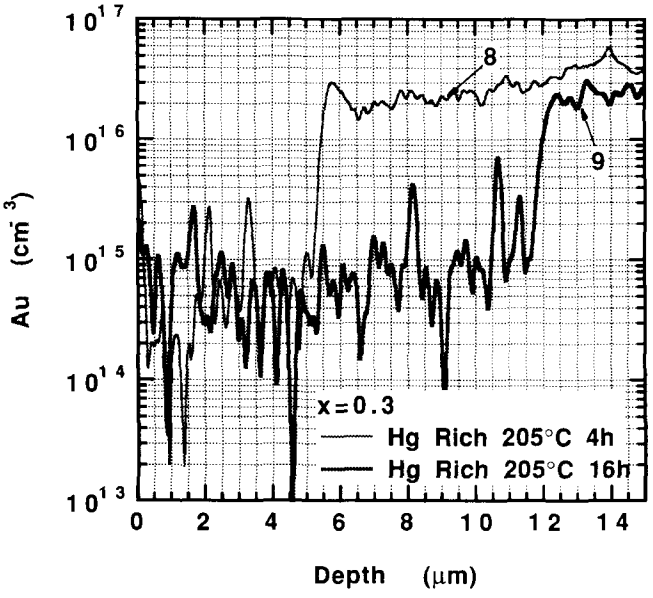

Fig. 3. Redistributed Au profiles for 205°C Hg anneals of 350°C Te equilibrated $Hg_{0.7}Cd_{0.3}Te$ for anneal times of 4 and 16 h. The sample numbers are identified in the figure and can be referenced in Table I.

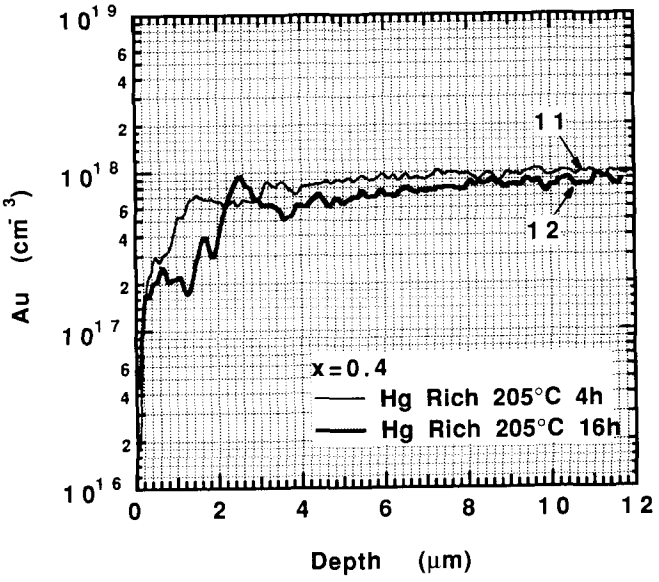

Fig. 4. Redistributed Au profiles for 205°C Hg anneals of 350°C Te equilibrated $Hg_{0.6}Cd_{0.4}Te$ for anneal times of 4 and 16 h. The Au/v_o ratio in this material is 22.5. The sample numbers are identified in the figure and can be referenced in Table I.

where the second term may always be neglected if $Au<<v_o$, but is not necessarily important when $Au>v_o$. Recall that if vacancies below the junction are the only net consumers of Au interstitials from the converted side, net Hg interstitials will come from the p-side to take part in the vacancy annihilation process. This occurs because recombination of Au interstitials through the Frank-Turnbol interaction lowers the vacancy concentration, which in turn drives the Frenkel reaction to generate additional vacancies and Hg interstitials to maintain equilibrium.

In using extrinsic impurities for understanding and quantifying formation processes, care must be exercised to ensure that the presence of the decorating impurity does not affect the interactions and resulting distributions of the intrinsic defects under study. An example of such an effect in $Hg_{0.8}Cd_{0.2}Te$ is demonstrated by Au SIMS profiles in Fig. 2a for a 175°C 1h Hg anneal and Fig. 2b for a 205°C 1h Hg anneal, as a function of the concentration of the decorating impurity. The initial background vacancy concentration was set by a Te-rich anneal at 300°C which results in a background vacancy concentration of roughly 4.8×10^{16} cm^{-3}.[2] The Au levels used for decoration were 9.8×10^{15} cm^{-3} and 2.4×10^{16} cm^{-3}. The Au to vacancy ratio (Au/v_o) is 0.2 and 0.5, respectively. Clearly, the junctions are shallower for the higher Au content indicating a $Au/v_o<0.5$ is required. Whether 0.2 is sufficient is still a question, though a look at the interstitial sink factor, f, yields further insight. The f values for all x = 0.2 samples are summarized in Table I, where the ($D_i i_R$) product was determined by using the SUMerCad simulator. For samples 1, 3, and 7, Au/v_o is ≤ 0.2 yielding an average f of 2.67. This is an indication that net Hg interstitials are being consumed by nonvacancy defects. For twice as much Au,

or $Au/v_o = 0.4$, the average f was 2.89; and for $Au/v_o = 0.5$, the average f was 4.64 for two samples. The saturation observed from 0.5 down to 0.2 indicates $Au/v_o \leq 0.2$ may be adequate for decoration. However, note that the apparent strong dependence of f on Au/v_o may be exaggerated by sample #2 which has an f seemingly inconsistently higher than the other samples. Neglecting this sample, a slope of 1 for f vs Au/v_o fits most of the data adequately. However, the limited data set is insufficient to determine whether or not f increases at a rate higher than a simple contribution from the additional Au lattice sites.

A more comprehensive set of experiments is necessary to understand the effect of Au/v_o on f, as well as to quantify what material properties (such as which extended defects) give rise to an f which is significantly greater than 1 for $Au/v_o << 1$.

Ambient Anneal Au Gettering (x = 0.3,0.4)

In this section, we will study the dependence of the Au redistribution in an initially uniform high vacancy background for MWIR and SWIR material following Hg-rich anneals; as a function of anneal time and temperature. As was found for the LWIR material in a previous study, the observed behavior of the low to high Au transition is consistent with that expected for type converted electrical junctions in vacancy-only material.[16]

We have studied the time dependence of Hg anneal induced Au redistribution in high vacancy uniformly Au-doped MWIR by comparing 4 and 16 h 205°C Hg-rich anneals of 350°C Te equilibrated material. The resulting Au distributions are shown in Fig. 3, and the experiment is summarized in Table I for samples 8 and 9. From Eq. (1), we expect the vacancy junction to go roughly as the square root of time for Hg anneals. Based on the kinetic models, we expect the vacancy junction to correspond approximately to the position of the steep Au rise. From Fig. 4, we estimate junction depths of 5.5 and 12.0 μm for the 4 and 16 h anneals, respectively. The depth ratio is 2.2, which compares well to two for square root [consistent with Eq. (1)], rather than four for linear. The f of these samples could not be determined since unlike $Hg_{0.8}Cd_{0.2}Te$, the D_i and i_R product has not been well established for $Hg_{0.7}Cd_{0.3}Te$. From interpolation of the phase limits in Fig. 1 between x = 0.2 and x = 0.4, we estimate the vacancy concentration following a 350°C Te equilibration anneal to be 8×10^{16} cm^{-3}. This yields a Au/v_o ratio of roughly 0.4 for all of the x = 0.3 samples. If we assume f is independent of composition and neglect electric field effects, then $(D_i\ i_R)$ is approximately 2.7×10^6 cm^{-1}/s using f = 2.89. In contrast, at 205°C $(D_i\ i_R)$ is 8.2×10^6 cm^{-1}/s in $Hg_{0.8}Cd_{0.2}Te$.

$Hg_{0.6}Cd_{0.4}Te$ samples were processed in the same manner as the two MWIR samples discussed above. The resulting Au distributions are shown in Fig. 4, and the experiment is summarized in Table I for samples 11 and 12. From Fig. 4, we determine junction depths of 1.0 and 2.05 μm for the 4 and 16 h anneals, respectively. The depth ratio is 2.05, which again compares favorably with the behavior predicted by Eq. (1). The f of these samples could not be determined since the D_i and i_R product has not been established for $Hg_{0.6}Cd_{0.4}Te$. From the phase limits in Fig. 1b, we estimate the vacancy concentration following a 350°C Te equilibration anneal to be 4×10^{16} cm^{-3}. This yields a Au/v_o ratio of roughly 22.5 for these samples. Based on extension of the dependence of f in LWIR material on the Au/v_o ratio, we would expect f to be quite large. If $(D_i\ i_R)$ for $Hg_{0.6}Cd_{0.4}Te$ at 205°C drops by the same factor in going from x = 0.3 to x = 0.4 as was observed from x = 0.2 to x = 0.3, $(D_i\ i_R)$ would equal 8.9×10^5 cm^{-1}/s and f would be 61, again neglecting electric field effects. However, for a firm determination of $(D_i\ i_R)$, the experiment will need to be repeated using a much lower Au concentration.

The temperature dependence of Hg anneal induced Au redistribution in high vacancy uniformly Au-doped $Hg_{0.7}Cd_{0.3}Te$ is shown in Fig. 5 comparing 205 and 225°C 4 h Hg-rich anneals of 350°C Te-equilibrated material. The experiment is summarized in Table I for samples 8 and 10. From Eq. (1), we can determine the ratio of $(D_i\ i_R)$ at the two temperatures. Using a junction depth ratio of 1.64, $(D_i\ i_R)$ at 225°C is found to be 7.2×10^6 cm^{-1}/s (again assuming f = 2.89 and neglecting electric field effects). We can determine an activation energy, and write,

$$D_i i_R(x = 0.3) = 9.3 \times 10^{16} \exp\left(\frac{-1.0\text{eV}}{kT}\right). \quad (3)$$

Recall that the Hg self-diffusion coefficient is given by,

$$D_{Hg} = \left(\frac{D_i i_R}{C_o}\right), \quad (4)$$

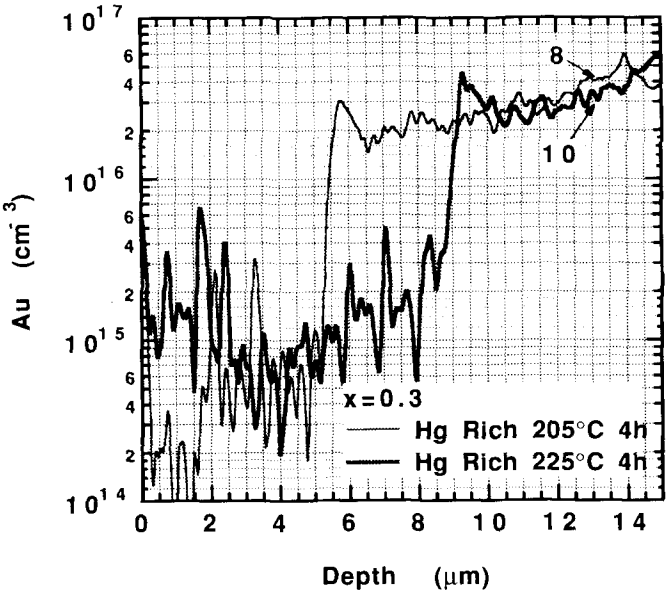

Fig. 5. Redistributed Au profiles for 4 h 205°C vs 225°C Hg anneals of 350°C Te equilibrated $Hg_{0.7}Cd_{0.3}Te$. The sample numbers are identi2fied in the figure and can be referenced in Table I.

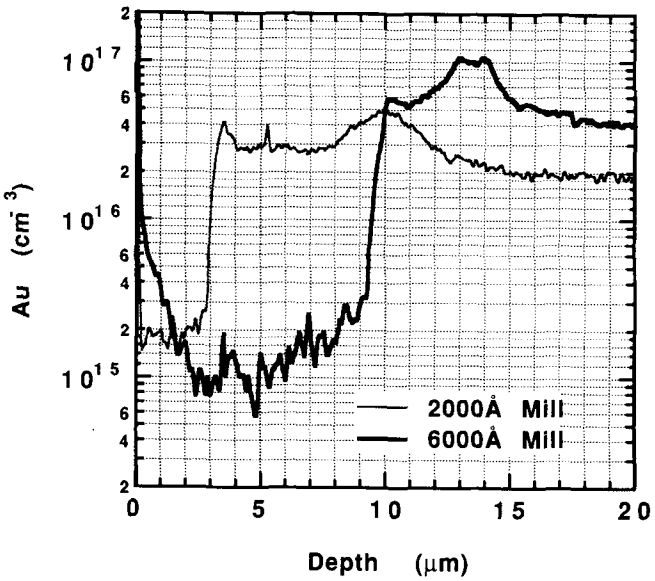

Fig. 6. Redistributed Au profiles for 2000 and 6000Å Ar mills of 350°C Te equilibrated $Hg_{0.7}Cd_{0.3}Te$.

where C_o is the density of Hg lattice sites.[13] The Hg self-diffusion coefficient for $Hg_{0.7}Cd_{0.3}Te$ is then given by,

$$D_{Hg}(x = 0.3) = 8.9 \times 10^{-6} \exp\left(\frac{-1.0eV}{kT}\right), \quad (5)$$

compared to,

$$D_{Hg}(x = 0.2) = 3 \times 10^{-3} \exp\left(\frac{-1.2eV}{kT}\right), \quad (6)$$

for $Hg_{0.8}Cd_{0.2}Te$.[3]

For $Hg_{0.7}Cd_{0.3}Te$, we determine $D_{Hg} = 1.9 \times 10^{-14}$ cm²/s at 307°C and 7.8×10^{-14} cm²/s at 352°C. The values for x = 0.2 material are 1.1×10^{-13} cm²/s and 6.4×10^{-13} cm²/s, respectively. This strong dependence of the Hg self-diffusion coefficient on composition compares favorably with that reported by Archer et al. in Fig. 5 of Ref. 3 for these two temperatures.

Ion Mill Au Gettering (x = 0.3)

In our previous work, we reported on the gettering of Au from low to high vacancy regions by an ion milling process.[16] For 300°C Te equilibrated $Hg_{0.8}Cd_{0.2}Te$, the type conversion observed was roughly 9.3 times the amount of material removed. Since the mill technique is a "kinetic" injection process vs the "thermodynamic" interstitial injection from a Hg ambient anneal, the compositional dependence of the type conversion rate by milling is not expected to be a strong function of composition. Secondary ion mass spectroscopy profiles are shown in Fig. 6 for 2000 and 6000Å mills of 350°C Te equilibrated $Hg_{0.7}Cd_{0.3}Te$. The junction depths are 3.2 and 9.8 μm, respectively, yielding a conversion rate of approximately 16 times the amount of material removed. This high conversion rate is an indication that the estimate of 8×10^{16} cm⁻³ for the vacancy concentration established by interpolation from the phase limits shown in Fig. 1 may be too high. Assuming the Hg interstitial injection rate is independent of composition implies a vacancy concentration of 2.8×10^{16} cm⁻³ for the 350°C x = 0.3 Te-rich anneal, which is closer to the x = 0.4 phase limits.

SUMMARY AND CONCLUSIONS

We have presented a number of experimental results aimed at increasing our understanding of cation impurity and native point defect diffusion and gettering mechanisms in $Hg_{1-x}Cd_xTe$. By studying Au gettering in $Hg_{0.8}Cd_{0.2}Te$ as a function of the Au/v_o ratio, it was established that trace amounts of the impurity are required to ensure that the "decorating" impurity does not in fact alter the apparent underlying intrinsic point defect distributions for a given type-conversion process. For both the MWIR and SWIR material, the Hg annealed gettered junction depth followed a square root of time dependence as predicted by the steady state model formalism. However, the Au/v_o ratios in these materials were dramatically different with estimates of 0.4 for the MWIR and 22.5 for the SWIR. The junction depths in the SWIR material were almost certainly governed by the high Au concentration. Finally, since the mill technique is a "kinetic" injection process vs the "thermodynamic" interstitial injection from a Hg ambient anneal, a weak compositional dependence of the mill Hg interstitial injection rate was found.

REFERENCES

1. H.R. Vydyanath, *J. Electrochem. Soc.* 128, 2609 (1981).
2. H.F. Schaake, *J. Electron. Mater.* 14, 513 (1985).
3. N.A. Archer, H.D. Palfrey and A.F.W. Willoughby, *J. Electron. Mater.* 22, 967 (1993).
4. N.A. Archer, H.D. Palfrey and A.F.W. Willoughby, *J. Cryst. Growth* 117, 177 (1992).
5. N. Archer and H. Palfrey, *J. Electron. Mater.* 20, 419 (1991).
6. Mei-Fan Sung Tang, Ph.D. Thesis, Stanford University (1987).
7. D.A. Stevenson and M-F.S. Tang, *J. Vac. Sci. Technol. B* 9, 1615 (1991).
8. M. Brown and A.F.W. Willoughby, *J. Cryst. Growth* 59, 27 (1982).
9. C.L. Jones, M.J.T. Quelch, P. Capper and J.J. Gosney, *J. Appl. Phys.* 53, (1982).
10. John-Sea Chen, Ph.D. Thesis, University of Southern California (1985).
11. D.T. Dutton, E. O'Keefe, P. Capper, C.L. Jones, S. Mugford and C. Ard, *Semicond. Sci. Technol.* 8, S266 (1993).
12. J.L. Meléndez and C.R. Helms, *J. Electron. Mater.* 24, 565 (1995).
13. J.L. Meléndez and C.R. Helms, *J. Electron. Mater.* 24, 573 (1995).
14. J.L. Meléndez, , Ph.D. Thesis, Stanford University (1993).
15. S. Holander, V. Sabnis, J. Hasan, J. Meléndez and C.R. Helms, *SUMerCad Process Simulator Software,* Stanford University (1994).
16. J.L. Meléndez, C.R. Helms, J. Tregilgas and J. Elkind, *SPIE* 228, 106 (1994).
17. H.R. Vydyanath and C.H. Hiner, *J. Appl. Phys.* 65, 3080 (1989).
18. R.F. Brebrick and J.P. Schwartz, *J. Electron. Mater.* 9, 771 (1980).
19. G.L. Hansen and J.L. Schmit, *J. Appl. Phys.* 54, 1639 (1983).
20. L.O. Bubulac, W.E. Tennant, R.A. Riedel, J. Bajaj and D.D. Edwall, *J. Vac. Sci. Technol. A* 1, 1646 (1983).
21. H.F. Schaake, J.H. Tregilgas, J.D. Beck, M.A. Kinch and B.E. Gnade, *J. Vac. Sci. Technol. A* 3, 143 (1985).